JOURNAL OF MATERIALS SCIENCE **35** (2000) 821–828

Weak beam observations of dissociation of pure screw dislocations in Ni_3Al

X. MENG*, A. R. PRESTON†
Department of Materials Science and Metallurgy, University of Cambridge, Pembroke Street, Cambridge, England
E-mail: xmeng@ccu.umanitoba.ca

The dissociation of superdislocations in Ni_3Al, which have a pure screw character, has been recorded on weak beam images at the **g**(5**g**) imaging condition. All screws were observed to dissociate on an {001} habit plane bounding APB faults. By computer modelling, the dissociation distance (d^{CSF}) of the Shockley partial dislocations that bound a complex stacking fault is shown to be less than 1.5 nm. This is the first reported case of fourfold dissociation bounding CSF+APB+CSF faults with a non-planar configuration and pure screw character. The energy values deduced from the measured spacing show quite large difference from the results obtained from dissociation with a planar system. It is questionable to use the linear anisotropic elasticity theory for such small splitting and nonplanar configuration. In addition our simulations demonstrate that a **g(ng)** condition is a wise choice for imaging partial separation.

1. Introduction

The measurement of fault energies for superdislocations with the fourfold dissociation have been reported for a number of Ni_3Al alloys [1–3]. Their results are all based on the planar configuration. So far the weak beam (as extrapolated from observations of edges) and HREM evidence we have on the sub-splitting of $1/2\langle 110\rangle$ partials all suggest that there is no visible sub-splitting of screw superpartials. The key technique in their work is the employment of an unusual 2**g**(5**g**) diffraction condition for the weak beam imaging at a range of electron energy from 150 kv to 300 kv. In addition they made use of a simulation program (CUFOUR, Schaublin and Stadelmann [4]) with a model including many-beam diffraction (Hirsch *et al.* [5]) and elastic anisotropy [6] calculations to correct for the effect of image peaks shifting from those of the cores. However, the interpretation of observations when using a 2**g** reflection will suffer from some difficulties. Here we are trying to give a picture for this problem by image simulations. Although these group of simulations do not represent a full assessment for the imaging conditions, they do generally show a possible mistake which can be made when using the 2**g**.

As indicated by Hemker and Mills [2] there may be more image peaks than dislocation cores; production of these supplementary peaks, was first addressed by Humphreys *et al.* [7], and experimentally observed by Hemker and Mills [2] in Ni_3Al using a 2**g** reflection. These results may cause some difficulties or confusion in the interpretation of experimental results. Hemker and Mills indicated from their simulations that the strongest pair of image peaks in fourfold-dissociated edges cannot be used in partial spacing measurement because they are independent of the spacing variation.

For a pure screw case, as simulations show in Fig. 1a(ii), at the **g**(5**g**) imaging condition, the number of partial image peaks directly agrees with the number of cores included in the model. Also the image contrast has a much simpler structure and makes local spacing measurement much simpler. It should be noted that both the right-hand and left-hand pairs of partial peaks shown in Fig. 1a(ii) can be used in the spacing measurement needed to deduce the CSF energy (based on the examination of simulations). In Fig. 1c the input value for d_{CSF} has been varied from 0.8 to 2 nm and the measured separations of each of the pairs for a given model spacing differ only slightly from each other. Further calculations have shown these differences depend on the foil normal and beam direction etc.

On the contrary at the 2**g**5**g** condition as shown in Fig. 1a(i) and the same dislocation configuration, it is much more difficult to measure the partial spacings directly because of the existence of extra image peaks whose positions and intensities are strongly dependent on imaging parameters. Our simulated images were performed at quite a high magnification (over 400 k and hence each point corresponds to an unphysically narrow column width) without any limitation of resolving power, and practically, there may be overlap among the peaks due to a lower image resolution. Further evidence is given in Fig. 1d and Fig. 1e showing the profiles of

* *Present address*: X. Meng, Department of Mechanical and Industrial Engineering, University of Manitoba, Winnipeg, Canada.
† *Present address*: A. Preston, Queen Mary College, University of London, London, England.

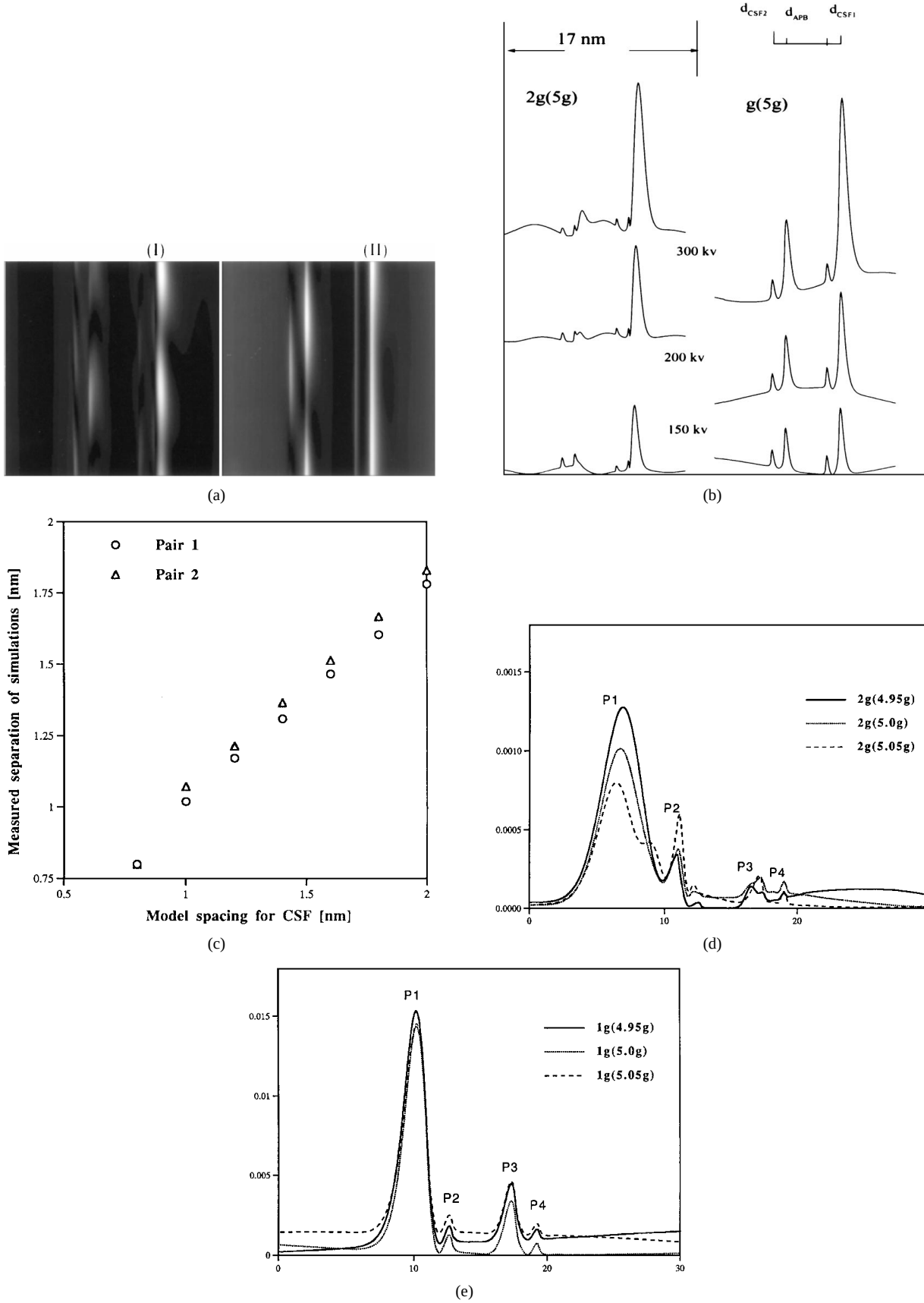

Figure 1 Comparison in image effects between the **g**(5**g**) and 2**g**(5**g**) conditions by simulations. a) Computer simulated images and peak profiles for a fourfold dissociated screw superdislocation in Ni_3Al (Beam direction = 113, Foil normal = 213, Foil thickness = 70 nm, $\mathbf{g} = 2\bar{2}0$). Simulated images at 200 kv and 2**g**(5**g**)(I) and **g**(5**g**)(II) conditions separately; b) Image peak profiles at conditions of 150 kV, 200 kV and 300 kV separately, showing the overlapping and contrast features at the 2**g**(5**g**)(I) and **g**(5**g**)(II) conditions separately and other imaging condition same as (a); It must be noted that intensities corresponding to pairs of the images at **g**(5**g**) and 2**g**(5**g**) conditions are not on the same scale while the intensities at different electron energies at the same reflection condition are because the intensities at 2**g**(5**g**) are over 5 times lower than the **g**(5**g**) condition; c) Image peak distances as a function of the input model at the **g**(5**g**) condition, showing both pairs can equally be useful for spacing measurement; the imaging condistions are the same with a)(II) at 200 kV (no projection correction); d) Computer simulated image peak profiles for a fourfold dissociated edge superdislocation in Ni_3Al (Beam direction = 113, Foil normal = 221, Foil thickness = 70 nm, $\mathbf{g} = 2\bar{2}0$) at 300 kV and 2**g**(5**g**); e) Peak profiles for dislocation the same as d) but imaging at 200 kV and **g**(5**g**).

image peaks for an edge superdislocation with fourfold dissociation using the 2**g**(5**g**) at 300 KV and the **g**(5**g**) reflection at 200 KV separately. The position marked "p3" may appear to be two peaks and the position for stronger one varies with slightly varying the deviation parameter (negative, exact and positive Bragg conditions) at the 2**g**(5**g**) condition while the p3 is stable and only one peak at **g**(5**g**) in simulations. The shift of the stronger "p3" between **2g(4.95g)** and **2g(5.0g)** conditions is about 0.7 nm which is rather significant for deducing fault energies. Baluc and Schaublin [3] have studied the correlation between the total six peaks and four Shockleys and assessed the relation between the appearance of the extra peak in p3 and partial spacings. Also, Baluc and Schaublin [3] made different interpretation for the strong pair (p1 and p2) from the conclusion by Hemker and Mills [2]. In Fig. 1d the p1 appears to be two peaks when there is one peak in p3 at the **g(5.05)** condition, so these demonstrate sufficiently the advantage of the **g**(5**g**) condition.

Here we have no intention to assess the general conditions when using the weak beam method in imaging very small separation. The purpose of this work is that firstly, we wish to examine critically the practicality of the application of the **g(ng)** condition to the measurement of partial spacings, and secondly, studies reported here show the fourfold dissociation with the cube APB/non-planar configuration, observed at the **g**(5**g**) weak beam condition. We try to use linear anisotropic elasticity to deduce the fault energy values associated with the measured spacings, and comment on the reliability of our results.

2. Experimental observations

2.1. Specimen preparation

The polycrystal of stoichiometric Ni_3Al used in the present study was supplied by Rolls Royce. The alloy was heat treated at 1000°C for 100 hours followed by a room temperature water quench. No deliberate deformation was performed and thin foils for TEM were prepared by electropolishing using a solution of 10% perchloric acid and 90% methanol at 15 V and −30°C.

The dislocations were imaged at 200 kV with a JEOL 2000 FX TEM, the magnification settings of which had been calibrated by HREM lattice imaging. The reflection vector ($\mathbf{g} = 220$) was chosen to be parallel to the overall Burgers vector $b_{\text{total}} = \text{a}[110]$ of the screw superdislocation. In order to set the weak beam **g(ng)** condition, the crystal was tilted in such a way that the Bragg condition was satisfied just past the nth fundamental diffracted beam. This diffraction resulted in a deviation parameter $s = 0.25\ \text{nm}^{-1}$ for the **g**(5**g**) condition.

It should be noted that using 200 kV rather than 300 KV is based on the consideration to minimize the specimen damage and to increase the visibility for weaker partials.

2.2. Observed dissociations

Fig. 2a represents a typical example of the frequently observed twofold dissociated superdislocation with a pure screw character, whose screw configurations were typically extremely straight and uniform on the scale of the resolution of the weak-beam images and were precisely aligned along [110].

In order to image any possible further dissociation of screws partials into CSF-coupled partial dislocations the beam direction was set to about [113] (midway between the (001) and (111) fault planes). All images at the **g**(4**g**) condition show only twofold dissociation. Higher deviation (above **g(6g)**) resulted in very low intensity of images. Fourfold dissociations were imaged, but only in a few cases, at the **g**(5**g**) condition at a magnification of 120 K or higher.

Fig. 2b shows the fourfold dissociation with very narrow spacing of the Shockley partials which are all aligned perfectly along [110]. Each pair of Shockley partials consists of a stronger peak alternating with a weaker peak. Fig. 2c shows the best image match obtained by simulation.

The distances between image peaks were measured using the image analysis program SEMPER to obtain peak profiles from digitized TEM negatives. For the twofold separations as shown in Fig. 2a, it is quite easy to make precise measurements either by projecting along whole dislocation length or by averaging a group of local measurements. For the fourfold dissociation the measurement of the apparent spacing is more difficult because of the faint intensity for the two weaker peaks, stronger overlapping between Shockley partial image profiles and oxide spots on the image caused by electron beam damage. Using SEMPER a number of local measurements have been made as shown in Fig. 2d, which were performed by projecting along short length segments. This procedure can effectively reduce noise in image peak profiles compared to isolated line scans.

A computer program with excellent peak-picking and curve-fitting algorithms which are based on Maximum Likelihood methods was used for fitting a model consisting of a set of peaks of various shapes, and baseline, to a given data set. This computing method could provide accurate positions of image peaks with corresponding confidence limits, of each component peak.

Fig. 2d shows an example of image peak profiles by projecting along a short length of the core near the foil centre and it also illustrates the curve-fitting method used to obtain the peak positions. Measurement of the peak separation at a series of positions along the dislocation length are given in Fig. 2e. Each point is from a line profile obtained by projecting along a length of a few nm. The apparent spacings obtained by averaging these points are shown in Table I which also gives input models for the calibration of image shift for the experimental results. The real spacings were obtained by matching the measured "apparent" separation to those generated by CUFOUR for different sets of core positions. They are considered to be a valid estimate assuming linear elasticity theory is valid. Comparisons of the simulated and the experimental values of spacings are given for both twofold and fourfold dissociations in Table I.

TABLE I Input data for the simulation (Fig. 1c), measured spacings from simulations and experiments for the two/four-fold dissociation of screw dislocations in Ni_3Al

	Partial spacing (nm)							
	Simulations					WB-observations		
	Input		Output					
		d_{APB}					d_{APB}	
Two-fold dissociation	4.75		4.39				4.40 ± 0.04	
	d_{CSF}	d_{APB}	d_{CSF2}	d_{APB}	d_{CSF1}	d_{CSF2}	d_{APB}	d_{CSF1}
Four-fold dissociation	1.4	4.34	1.32	3.83	1.38	1.25 ± 0.20	3.83 ± 0.27	1.38 ± 0.20

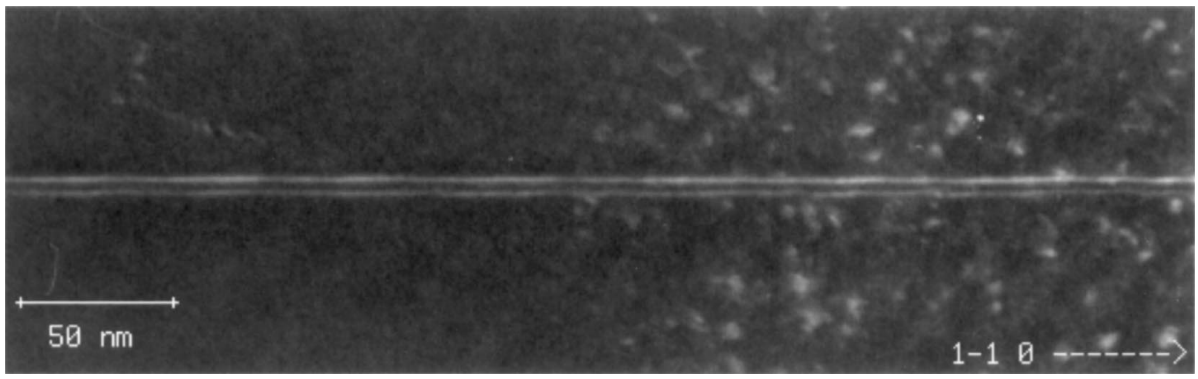

(a)

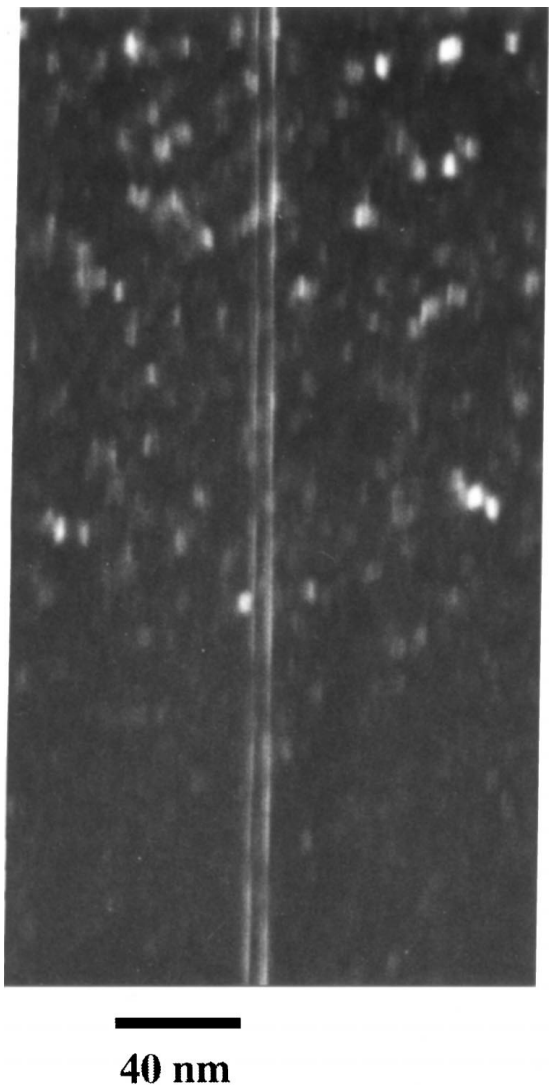

(b)

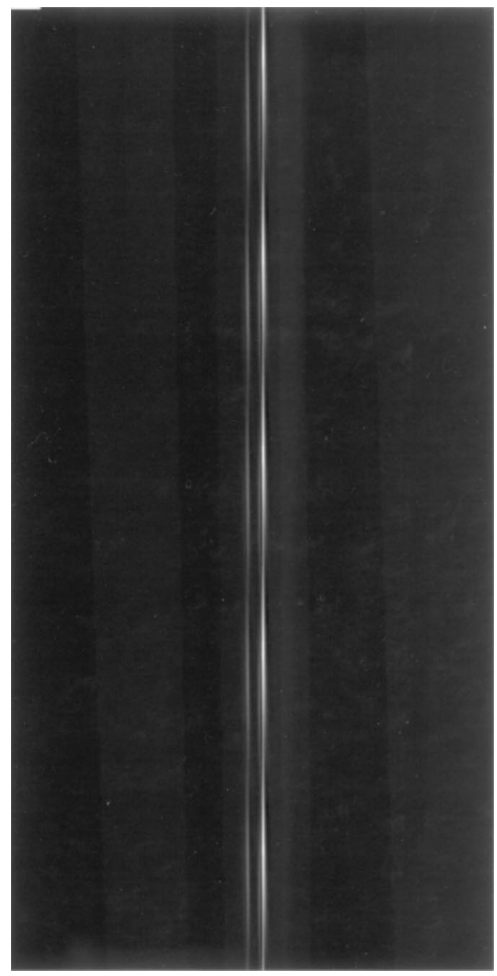

(c)

Figure 2 a) WB-TEM micrograph for twofold dissociated screw superdislocation showing perfect straight and uniform separation along the $1\bar{1}0$. b) Experimental micrograph at the **g**(5**g**) condition (Beam normal = 113, Foil normal = 3 2 14, thickness = 60 nm, HV = 200 kV); c) Simulated image for matching the experiment as shown in Fig. 2b); d) Example of Peak fitting for accurate determination of image peak positions in Fig. 2b; e) Data scattering plot from selected segments along the dislocation length from the fourfold dissociated dislocation in Fig. 2b.x. (*Continued*)

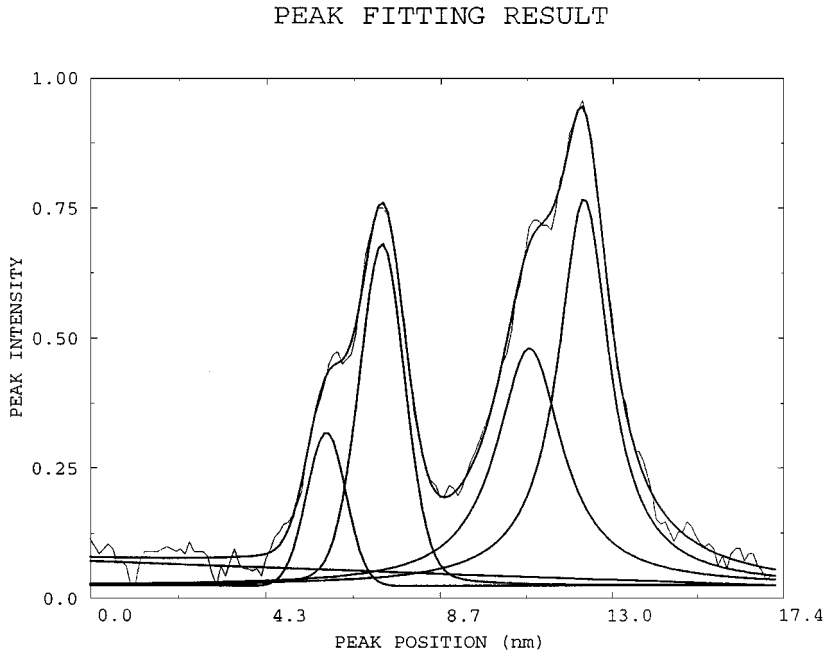

(d)

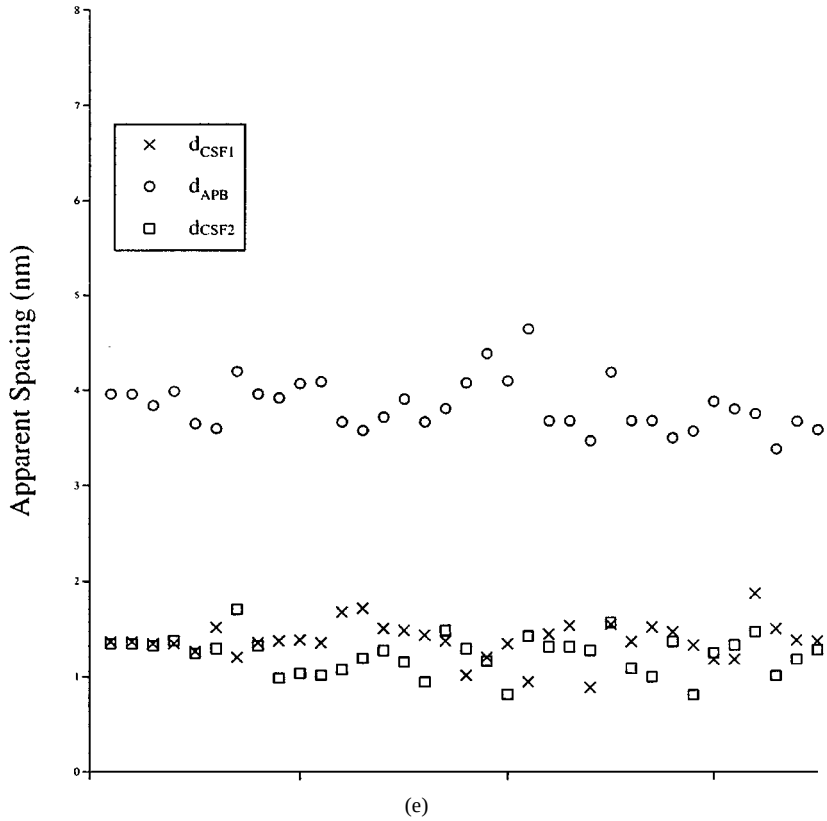

(e)

Figure 2 (*Continued*).

3. Energy deduction

As described by Vanderschaeve [8] for a planar configuration of fourfold dissociation there are two equilibrium equations:

$$\gamma_{\mathrm{CSF}} = \frac{f_{12}}{d_{\mathrm{CSF}}} + \frac{f_{11}}{d_{\mathrm{APB}} + d_{\mathrm{CSF}}} + \frac{f_{12}}{d_{\mathrm{APB}} + 2d_{\mathrm{CSF}}} \quad (1)$$

$$-\gamma_{\mathrm{CSF}} + \gamma_{\mathrm{APB}} = -\frac{f_{21}}{d_{\mathrm{CSF}}} + \frac{f_{21}}{d_{\mathrm{APB}}} + \frac{f_{22}}{d_{\mathrm{APB}} + d_{\mathrm{CSF}}} \quad (2)$$

where f_{ij} is the energy factor and γ is the fault energy. The energy factors can be calculated from Stroh's model [6] in which only the radial force need be considered. By computer atomistic simulation Yamaguchi *et al.* [9] show that if the superdislocation splitting involves APB on a single 111 plane the cores of the corresponding superpartials are likely to be planar, confined to this 111 plane and may be described as dissociated into corresponding Shockley partials and therefore this dislocation is expected to be glissile with low Peierls stress, analogous to the twofold dissociated dislocation in f.c.c metals. In using Equations 1 and 2 for case of Ni_3Al, we obtained 1.67 as the value for the ratio of separation of the edge and the screw superpartials lying

on (111) bounding an APB fault (twofold dissociation) which is the same as Yoo's work [10]. In our calculations the ratio of the splitting of partials separated by a CSF fault between pure edge and pure screw is 2.27 while the similar ratio for partials separated by an APB is 1.67 the same as the twofold dissociation case. These results are also obtained by Hemker and Mills [2]. It should be noted that all our elastic calculations are performed by a computer subroutine: ANCALC developed by Head *et al*. [11] which includes the algorithm for Stroh's model [6].

For the non-planar or Kear-Wilsdorf configuration as shown in Fig. 3 we have:

$$[1\bar{1}0] \rightarrow \underbrace{\frac{1}{6}[1\bar{2}1]}_{\text{CSF(111)}} + \underbrace{\frac{1}{6}[2\,\overline{1}\,\overline{1}]}_{\text{APB(001)}} + \underbrace{\frac{1}{6}[1\,\bar{2}\,1]}_{\text{CSF(111)}} + \frac{1}{6}[2\overline{1}\overline{1}]$$

The relation between dislocation widths and the fault energies is:

$$\gamma_{\text{CSF}} = \frac{f_{12}}{d_{\text{CSF}}} + \frac{f_{11}}{r_2}\cos(\alpha_0 - \alpha_2)\frac{f'_{11}}{r_2} \times \sin(\alpha_0 - \alpha_2) + \frac{f_{12}}{r_1}\cos(\alpha_0 - \alpha_1) + \frac{f'_{12}}{r_1}\sin(\alpha_0 - \alpha_1) \quad (3)$$

$$-\gamma_{\text{CSF}} + \gamma_{\text{APB}} = -\frac{f_{12}}{d_{\text{CSF}}} + \frac{f_{21}}{d_{\text{APB}}}\cos\alpha_0 + \frac{f'_{21}}{d_{\text{APB}}}\sin\alpha_0 + \frac{f_{22}}{r_2}\cos\alpha_2 + \frac{f'_{22}}{r_2}\sin\alpha_2 \quad (4)$$

where f'_{ij} represents the component corresponding to tangential force and the full derivation was given by Stroh [6] and provided in using the elasticity theory valid. These equations appear more complicated than the planar case because the tangential component of the force has also to be considered. Using ANCALC we can easily obtain the parameters needed for the non-planar configuration (Fig. 3). Expression (4) is given under the assumption that the two inner partials can move along {111} plane rather than {001}.

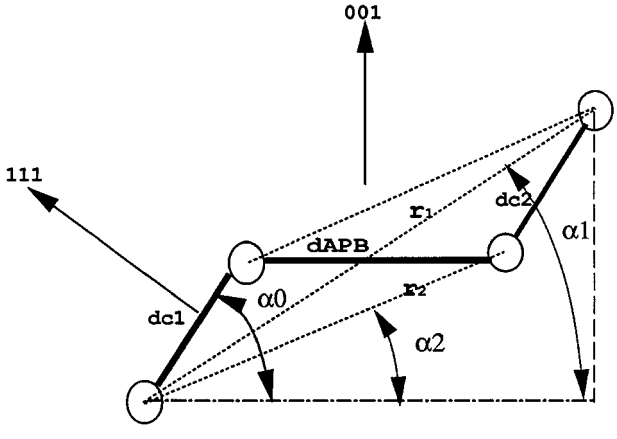

Figure 3 Diagram of non-planar configuration of a fourfold dissociation in Ni_3Al (dislocation line sense is perpendicular to the paper).

Using partial separation in Table I and Equations 1–4 the energy values deduced for twofold dissociation is $\gamma_{\text{APB}_{001}} = 146 \pm 2$ erg/cm^2 while for the fourfold dissociation $\gamma_{\text{APB}_{001}} = 122 \pm 9$ erg/cm^2 and $\gamma_{\text{CSF}} = 112 \pm 8$ erg/cm^2.

4. Discussion

Data in Table I shows both the simulated and experimental Shockley partial spacings ($d_{\text{CSF1}}, d_{\text{CSF2}}$) are slightly asymmetrical. Considering the data scattering feature by the weak beam method the asymmetry in the experimental work is thought an image shift effect rather than existence of a physical difference between the two pair partials. This conclusion obeys the assumption by Vanderschaeve [8].

We have obtain a good match in image contrast between the TEM micrograph (Fig. 2b) and the simulation (Fig. 2c), which means that only the simulations based on the CSF+APB+CSF dissociation mode and parameters in Table I can agree with the observed fourfold image. This is also based on the fact that the possible dissociations observed by different workers in this alloy system are the twofold APB fault (either planar 111 or non-planar 001 types), the fourfold CSF + APB + CSF fault configuration and super intrisic fault that can be determined by the routine Burgers analysis. In addition, the relative peak strength among the partial peak intensities for fourfold dissociation is not varied with varying the imaging conditions revealed by previous studies [2] and [3], and the image simulations by us, for example, the image simulations show that four partials always have the peak intensity configuration as strong + weak + strong + weak as demonstrated in Fig. 1bII at **g**(**ng**) conditions, never emerging in a form of strong+strong+weak+weak or strong+weak+weak+strong or other kind of configurations.

The comparison in Fig. 2b and Fig. 2c demonstrates that, as predicted by the simulations, the image peaks have a much simpler structure than those seen previously using the 2**g**(5**g**) condition. Although the image resolution for our experiments is poorer than those using the 2**g**(5**g**) condition, the apparent spacing we achieved is less 1.5 nm which is the level obtained by Hemker and Mills [2], and Baluc and Schaublin [3]. We are not surprised that both of the two groups obtained over 40% image shift for two tenary addition alloys. Hemker and Mills [2] gave 16% image shift for the Ni76Al alloy and we have about 10%. This is because the image shift effect is different for faults on cube and octehedral planes. The Fig. 4 shows that relation between model and measurement from our image simulations for a screw superdislocation lying on (001). Obviously, the shift for a cube APB is rather small when the model spacing is larger than 4 nm and may be ignorable when spacings are larger than 5 nm. For cases of faults on (111) the shift effect is relatively much larger which can be seen from the results obtained by Stobbs and Sworn [12] in Cu, Hemker and Mills [2] in Ni_3Al. It must be noted that the correction we used is different from the classic Cockayne correction [13] in which the image shift is independent on the fault habit planes.

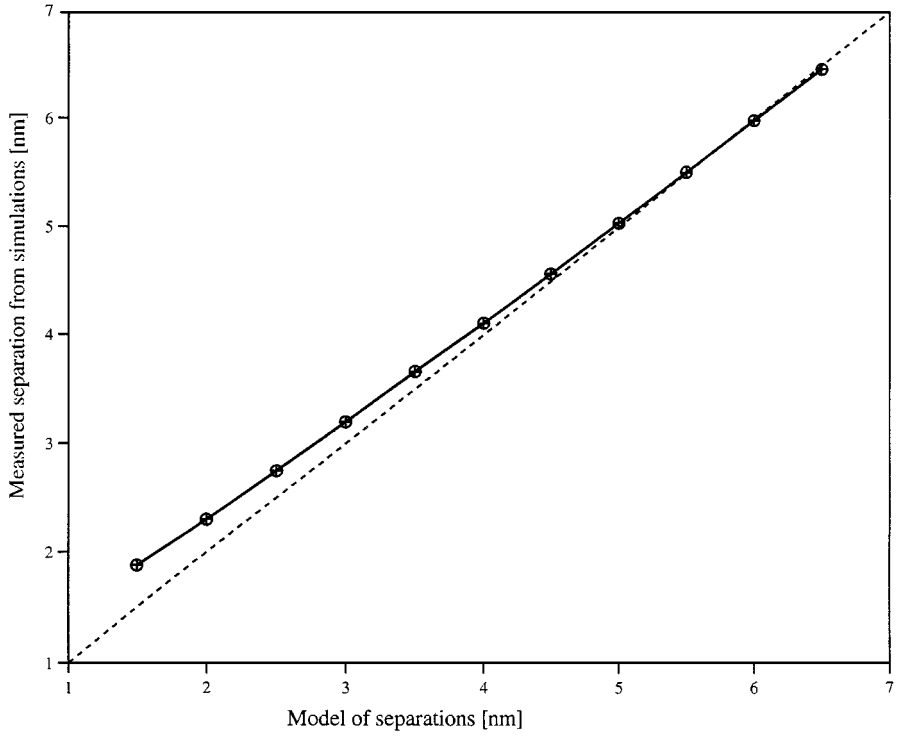

Figure 4 Correlation between the measured separation from simulated images of a twofold screw APB on (001) and the input models; beam direction = 116 at **g**(4**g**), 200 kV, non-beam convergence (no projection correction for the inclined fault).

Schaublin *et al.* [14] and Meng *et al.* [15] indicated that deviation and the beam convergence are most important parameters in controlling the measurement of partial spacings. If the deviation is sufficiently large the effects of the beam convergence can also be ignored. For Ni_3Al at 200 kV and a 220 type of reflection (**g**(5**g**)) Meng *et al.* [15] by simulations show that the beam convergence effect is small. In practise, the image visibility for weakest partials is much more important factor than others. The quality of a high resolution weak beam image will be determined by a combination of various imaging parameters, which is difficult to give a general guide by simulations. We do not suggest never to use the 2**g**(5**g**) reflection but it does need to take great care to the peak positions in interpretation of results when using it.

The most surprised in our results is the CSF energy being lower than the APB fault energy which is thought to be unusual. There are several points which may influence our interpretation and measurement:

- As suggested by Yamaguchi *et al.* (1981, 1982) [9], the non-planar configuration of stacking fault can not be treated as a case of fcc structure;
- Shockleys were broader introduced by segregation.

For the last point, we must indicate that the ordering phase of the specimen is very stable up to over 1600 K*, so the studied alloy is quite homogeneous in chemistry.

Another question is about the validity of the elastic model when derived from narrowly separated Shockleys and the measured CSF energies can significantly deviate from the true CSF energy. The discussion for this problem have been given by Stobbs and Sworn [12].

It is very hard to make accurate comparison with other measurements because of differences in the imaging condition, correction method and alloy chemistry. However, the ratio between the CSF and APB energies should be larger than one, which is thought a general property for L_{12} alloys. The results from Hemker and Mills [2], and Baluc and Schaublin [3] all have a "positive" ratio between the CSF and APB energies. From this point, our deduced CSF fault energy is so different and it is very likely the non-planar configuration play a major role for elastic model breaking down for the fourfold dissociation.

5. Conclusion

1. Computer simulations show that the **g**(n**g**) reflection condition has at lwast an advantage over the 2**g**(n**g**) condition (no supplementary (ghost) peaks). Our experiment demonstrates that **g**(n**g**) condition can be used even for very narrow separations;

2. The appropriateness of using linear elasticity is doubtful for narrow splittings in a non-planar configuration;

3. A value of $\gamma_{\mathrm{APB}_{001}} = 146 \pm 2$ erg/cm^2 is obtained from the twofold dissociated superdislocations.

Acknowledgement

XM acknowledge the C. C. Wu foundation of Hong Kong for financial support. Rolls-Royce is acknowledged for supplying the speciment used in this study. We thank Professors C. J. Humphreys and A. H. Windle for the provision of laboratory facilities.

* According to Equilibrium Plot supplied by Rolls-Royce.

References

1. N. BALUC, H. P. KARNTHALER and M. J. MILLS, *Phil. Mag A* **64** (1991) 137.
2. K. HEMKER and M. MILLS, *ibid.* **68** (1993) 305.
3. N. BALUC and R. SCHAUBLIN, *ibid.* **74** (1996) 1113.
4. R. SCHAUBLIN and P. STANDELMANN, *Materials Science and Engineering A* **164** (1993) 373.
5. P. B. HIRSCH, A. HOWIE, R. B. NICHOLSON, D. W. PASHLEY and M. J. WHELAN, "Electron Microscopy of Thin Crystals" (London, Butterworths, 1965), p. 229.
6. A. H. STROH, *Phil. Mag.* **3** (1958) 625.
7. C. J. HUMPHREYS, R. A. DRUMMOND and A. HARTDAIVS, *Phil. Mag. A* (1977) 1543.
8. G. VANDERSCHAEVE, *ibid.* **56** (1987) 689.
9. M. YAMAGUCHI, V. VITEK and D. P. POPE, *ibid.* **43** (1981) 1027; M. YAMAGUCHI, V. PAIDAR, D. P. POPE and V. VITEK, *ibid.* **45** (1982) 869.
10. M. H. YOO, *Acta Metall.* **35** (1987) 1559.
11. A. K. HEAD, P. HUMBLE, L. CLAREBROUGH, A. J. MORTON and C. T. FORWOOD, "Computed Electron Micrographs and Defect Identification" (North-Holland, Amsterdam, 1973).
12. W. M. STOBBS and S. SWORN, *Phil. Mag. A* **17** (1971) 1710.
13. D. J. H. COCKAYNE, in "Diffraction and Imaging Techniques in Material Science," edited by S. Amelinckx et al. (North-Holland Publishing Company, Amsterdam, 1978) p. 174.
14. R. SCHAUBLIN, X. MENG and W. M. STOBBS, *Inst Phys. Conf: EMAG* **147** (1995) 91.
15. X. MENG, R. SCHAUBLIN and W. M. STOBBS, *Phil. Mag Lett.* **75** (1997) 179.

Received 2 March
and accepted 16 August 1999